PERFECT MATCHING OF ULTRAHIGH-BRIGHTNESS BEAMS IN VARIABLY FOCUSED CHANNELS*

Renato Pakter, UFRGS, Porto Alegre, RS, Brazil
Chiping Chen, MIT, Cambridge, MA, USA

Abstract

It is shown that there exists a new class of cold-fluid corkscrewing elliptic beam equilibria for ultrahigh-brightness, space-charge-dominated beam propagation through a linear focusing channel consisting of uniform solenoidal, periodic solenoidal, and/or alternating-gradient quadrupole focusing magnets in an arbitrary arrangement including field tapering. As an important application of the present equilibrium beam theory, a general technique is developed to control large-amplitude density and flow velocity fluctuations (such as beam hollowing and halo formation) often observed in ultrahigh-brightness beams.

1 INTRODUCTION

One of the key mechanisms for halo formation in high-intensity electron or ion beams is due to a mismatch in the particle phase-space distribution relative to an equilibrium distribution. In general, distribution mismatch can lead to rather complex evolution in a beam, including not only halo formation but also beam hollowing. This mechanism for halo formation and beam hollowing occurs for rms matched beams because rms beam matching does not necessarily guarantee the beam in an equilibrium state.

Both halo formation and beam hollowing were observed in the heavy ion beam injector experiment at LBNL [1], in which an ultrahigh-brightness, space-charge-dominated potassium ion beam was generated with an axisymmetric Pierce diode and then accelerated by a set of electrostatic quadrupoles.

In this paper, we present exact steady-state solutions to the cold-fluid equations governing the evolution of an ultrahigh-brightness, space-charge-dominated beam propagating through a linear focusing channel. As an important application of the equilibrium beam theory, we develop and demonstrate a technique for controlling of beam halo formation and beam hollowing in ultrahigh-brightness beams.

2 THEORETICAL MODEL

We consider a thin, continuous, ultrahigh-brightness, space-charge-dominated beam propagating with constant axial velocity $\beta_b c\hat{\mathbf{e}}_z$ through a linear focusing channel with multiple periodic solenoidal and alternating-gradient quadrupole focusing sections. The focusing fields can Be be tapered, and the quadrupoles are allowed to be at various angles in the transverse direction. The focusing magnetic field is approximated by

$$\mathbf{B}_0(\mathbf{x}) = B_z(s)\,\hat{\mathbf{e}}_z - \frac{1}{2}B_z'(s)\left(x\hat{\mathbf{e}}_x + y\hat{\mathbf{e}}_y\right) + \left(\partial B_{\bar{x}}^q/\partial\bar{y}\right)_0\left(\bar{y}\,\hat{\mathbf{e}}_{\bar{x}} + \bar{x}\,\hat{\mathbf{e}}_{\bar{y}}\right), \tag{1}$$

where $B_z'(s) = (\partial B_z/\partial s)_0$, $s = z$ is the axial coordinate, $\bar{x}$, $\bar{y}$, $\hat{\mathbf{e}}_{\bar{x}}$, and $\hat{\mathbf{e}}_{\bar{y}}$ are coordinates and unit vectors of a frame of reference that is rotated by an angle of φ_q with respect to the x-axis in the laboratory frame, $\left(\partial B_{\bar{x}}^q/\partial\bar{y}\right)_0 = \left(\partial B_{\bar{y}}^q/\partial\bar{x}\right)_0$, and the subscript 'zero' denotes $(x, y) = 0 = (\bar{x}, \bar{y})$.

For an ultrahigh-brightness beam, kinetic (emittance) effects are negligibly small, and the beam can be adequately described by cold-fluid equations. In the paraxial approximation, the steady-state cold-fluid equations for time-stationary flow $(\partial/\partial t = 0)$ are

$$\beta_b c\frac{\partial}{\partial s}n_b + \nabla_\perp\cdot\left(n_b\mathbf{V}_\perp\right) = 0, \tag{2}$$

$$\nabla_\perp^2\phi^s = \beta_b^{-1}\nabla_\perp^2 A_z^s = -4\pi q n_b, \tag{3}$$

$$n_b\left(\beta_b c\frac{\partial}{\partial s} + \mathbf{V}_\perp\cdot\frac{\partial}{\partial\mathbf{x}_\perp}\right)\mathbf{V}_\perp = \frac{qn_b}{\gamma_b m}\left[-\frac{1}{\gamma_b^2}\nabla_\perp\phi^s + \beta_b\hat{\mathbf{e}}_z\times\mathbf{B}_{0\perp} + \frac{\mathbf{V}_\perp}{c}\times B_z(s)\hat{\mathbf{e}}_z\right], \tag{4}$$

where $\mathbf{x}_\perp = x\hat{\mathbf{e}}_x + y\hat{\mathbf{e}}_y$, $\gamma_b = \left(1-\beta_b^2\right)^{-1/2}$, and the self-electric and self-magnetic fields $\mathbf{E}^s$ and $\mathbf{B}^s$ are determined from the scalar and vector potentials ϕ_s and $A_z^s\hat{\mathbf{e}}_z$, i.e., $\mathbf{E}^s = -\nabla_\perp\phi^s$ and $\mathbf{B}^s = \nabla\times A_z^s\hat{\mathbf{e}}_z$.

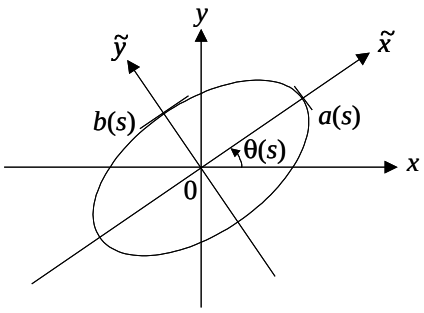

Fig. 1: Laboratory and rotating coordinate systems.

*Work supported by USDOE, AFOSR, and CNPq, Brazil.

3 CORKSCREWING BEAM EQUILIBRIUM

We seek solutions to Eqs. (2)-(4) of the form

$$n_b(\mathbf{x}_\perp, s) = \frac{N_b}{\pi a(s) b(s)} \Theta\left[1 - \frac{\tilde{x}^2}{a^2(s)} - \frac{\tilde{y}^2}{b^2(s)}\right], \tag{5}$$

$$\mathbf{V}_\perp(\mathbf{x}_\perp, s) = [\mu_x(s)\tilde{x} - \alpha_x(s)\tilde{y}]\beta_b c\hat{\mathbf{e}}_{\tilde{x}} + [\mu_y(s)\tilde{y} + \alpha_y(s)\tilde{x}]\beta_b c\hat{\mathbf{e}}_{\tilde{y}}. \tag{6}$$

In Eqs. (5) and (6), $\mathbf{x}_\perp = \tilde{x}\,\hat{\mathbf{e}}_{\tilde{x}} + \tilde{y}\,\hat{\mathbf{e}}_{\tilde{y}}$ is a transverse displacement in a rotating frame illustrated in Fig. 1; $\theta(s)$ is the angle of rotation of the ellipse with respect to the laboratory frame; and $\Theta(x)$ = 1 if $x > 0$ and $\Theta(x) = 0$ if $x < 0$.

Substituting Eqs. (5) and (6) in Eqs. (2)-(4) we obtain the generalized beam envelope equations [2]

$$\frac{d^2a}{ds^2} + \{\kappa_q(s)\cos[2(\theta - \varphi_q)] - \frac{b^2(\alpha_x^2 - 2\alpha_x\alpha_y) + a^2\alpha_y^2}{a^2 - b^2} - 2\alpha_y\sqrt{\kappa_z}\}a - \frac{2K}{(a+b)} = 0,$$

$$\frac{d^2b}{ds^2} + \{-\kappa_q(s)\cos[2(\theta - \varphi_q)] + \frac{a^2(\alpha_y^2 - 2\alpha_x\alpha_y) + b^2\alpha_x^2}{a^2 - b^2} - 2\alpha_x\sqrt{\kappa_z}\}b - \frac{2K}{(a+b)} = 0,$$

$$\frac{d}{ds}\left[b^2(\alpha_x + \sqrt{\kappa_z})\right] - \frac{a^3b(\alpha_x - \alpha_y)}{a^2 - b^2}\frac{d}{ds}\left(\frac{b}{a}\right) + \kappa_q(s)b^2\sin[2(\theta - \varphi_q)] = 0, \tag{7}$$

$$\frac{d}{ds}\left[a^2(\alpha_y + \sqrt{\kappa_z})\right] - \frac{ab^3(\alpha_x - \alpha_y)}{a^2 - b^2}\frac{d}{ds}\left(\frac{a}{b}\right) - \kappa_q(s)a^2\sin[2(\theta - \varphi_q)] = 0,$$

$$\frac{d\theta}{ds} - \frac{a^2\alpha_y - b^2\alpha_x}{a^2 - b^2} = 0,$$

$$\mu_x = \frac{1}{a}\frac{da}{ds}, \qquad \mu_y = \frac{1}{b}\frac{db}{ds}.$$

Equations (7), together with the density and velocity profiles defined in Eqs. (5) and (6), describe cold-fluid equilibrium states for variably focused ultrahigh brightness beams.

4 PERFECT MATCHING OF ULTRAHIGH-BRIGHTNESS BEAMS

As an important application of the equilibrium beam theory, we develop and demonstrate a technique for controlling of beam halo formation and beam hollowing in ultrahigh-brightness beams. This technique is widely applicable in the design of ultrahigh-brightness beams, and is effective before any collective instability develops to reach considerably large amplitudes.

To demonstrate the efficacy of this technique, we consider here a specific example, namely, the matching of a round particle beam generated by an axisymmetric particle source into alternating-gradient magnetic quadrupole focusing channel. For comparison, we analyze two non-rotating rms matched beams with the same intensity; one beam will be in equilibrium and the other beam has an initial perturbation about the equilibrium transverse flow velocity. At the entrance of the alternating-gradient magnetic focusing channel $(s = 0)$, both beams have the same density profile defined in Eq. (5), but the transverse flow velocities of the beams are of the form

$$\frac{d\mathbf{x}_\perp}{ds} = \frac{\mathbf{x}_\perp}{a}\left(\frac{da}{ds}\right)\left[1 + \nu\left(1 - \frac{2\mathbf{x}_\perp \cdot \mathbf{x}_\perp}{a^2}\right)\right], \tag{8}$$

where ν is a parameter that measures the nonlinearity in the velocity profile. For example, an initial velocity profile with $\nu > 0$ in Eq. (8) may model the effects of the concave shape of a Pierce-type ion diode in the LBNL 2-MV Heavy Ion Beam Injector Experiment [1]. The value of ν in the LBNL experiment is estimated to be $\nu = 0.25$. For equilibrium beam propagation, $\nu = 0$.

The rms matching for both beams with $\nu = 0$ and 0.25 is obtained by numerically solving the rms envelope equations [3]

$$\frac{d^2\bar{a}}{ds^2} + \kappa_q(s)\bar{a} - \frac{K}{2(\bar{a} + \bar{b})} = 0, \tag{9a}$$

$$\frac{d^2\bar{b}}{ds^2} - \kappa_q(s)\bar{b} - \frac{K}{2(\bar{a} + \bar{b})} = 0, \tag{9b}$$

where $\bar{a} \equiv \langle x^2 \rangle^{1/2}$ and $\bar{b} \equiv \langle y^2 \rangle^{1/2}$ are the rms envelopes, $\langle \cdots \rangle$ denotes average over the particle distribution, and emittance terms are neglected. For given

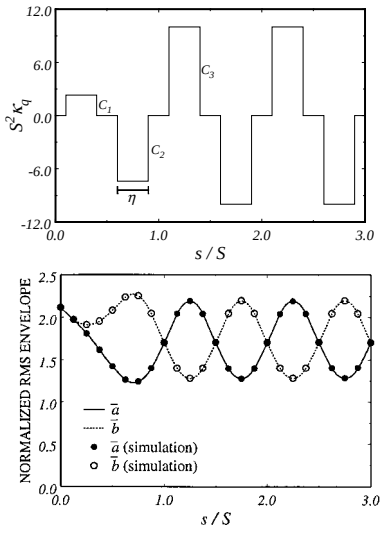

Fig. 2: Focusing field parameter and matched envelopes

beam intensity K and focusing channel parameters C_3 and η shown in Fig. 2, we make use of Eq. (9) to determine the injection parameters for the axisymmetric beam, namely, $\bar{a}(0)$, $\bar{b}(0)$, $\bar{a}'(0)$ and $\bar{b}'(0)$, as well as the strengths of the two quadrupoles centered at $s = S/4$ and $s = 3S/4$ in the first lattice, C_1 and C_2, as shown in Fig. 2 [2]. The results are presented in Fig. 2 which show, respectively, the focusing field parameter $S^2\kappa_q$ and the rms matched envelopes $\bar{a}(s)$ and $\bar{b}(s)$ as a function of s for the focusing channel with vacuum phase advance $\sigma_0 = 70.8^\circ$ and beam perveance $SK/4\varepsilon(0) = 16.0$, where a negligibly small unnormalized rms emittance of $\varepsilon(0) = 0.15\times10^{-6}$ m-rad has been assigned to the beam at $s = 0$.

Self-consistent simulations are performed with $N_p = 3072$ and free-space boundary conditions to study the phase space evolution for the two beams in the focusing channel. In Fig. 2, the solid dots and open circles correspond to the rms envelopes $\bar{a}(s)$ and $\bar{b}(s)$ obtained from a self-consistent simulation for a beam initially with a nonlinear velocity profile with $\nu = 0.25$. It is evident in Fig. 2 that there is excellent agreement between the prediction of the rms envelope equations (9a) and (9b) and the results of the self-consistent simulation, despite that the transverse flow velocity is perturbed substantially.

We now examine the evolution of the particle distribution if the nonlinearity in the initial transverse flow velocity profile is introduced, and compare with equilibrium beam propagation. The results are summarized in Figs. 3 and 4. Figure 3 shows a comparison between particle distributions in the configuration space with and without nonlinearity in the initial transverse flow velocity at three axial positions: $s/S = 0$, 1.0 and 2.5. These axial positions are chosen such that $\bar{a}(s) = \bar{b}(s)$. In Fig. 3, the plots shown on the left correspond to $\nu = 0$ and those on the right to $\nu = 0.25$. For $\nu = 0.25$, the initially round beam develops sharp edges after the first lattice, becoming partially hollow subsequently at $s/S = 2.5$. In Fig. 4(b), the radial distribution of 3072 macroparticles at $s/S = 2.5$ shows that the density at the edge is twice the density at the center of the beam, and that there is a small halo extending outward beyond the radius where the density reaches its maximum. The partially hollow density profile shown in Fig. 4(b) is similar to, but not as pronounced as, that observed in the heavy ion beam injector experiment at LBNL [1]. In contrast to the case with $\nu = 0.25$, the beam propagates in an equilibrium state for $\nu = 0$ without beam hollowing and without any significant beam halo formation, as shown in Fig. 4(a).

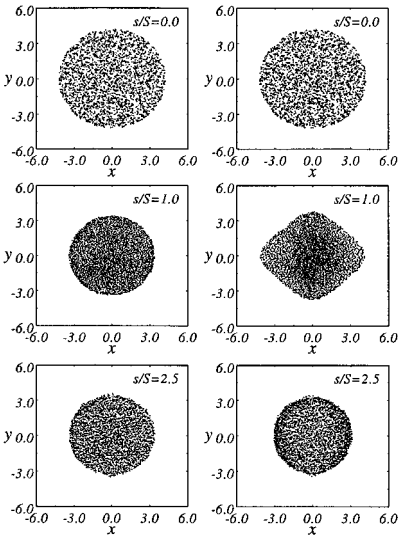

Fig. 3: Particles distribution for ν=0 (left) and ν=0.25 (right).

5 SUMMARY

We presented exact steady-state solutions to the cold-fluid equations governing the evolution of an ultrahigh-brightness beam propagating through a linear focusing channel. As an important application of the equilibrium beam theory, we developed and demonstrated a technique for controlling of beam halo formation and beam hollowing in ultrahigh-brightness beams.

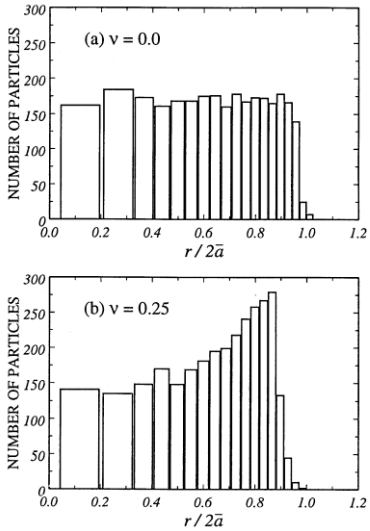

Fig. 4: Beam density profiles at *s/S*=2.5.

REFERENCES

[1] S. Yu, S. Eylon, E. Henestroza, and D. Grote, AIP Conf. Proc. **377**, 134 (1996).

[2] R. Pakter and C. Chen, Phys. Rev. E, to appear (2000).

[3] F. J. Sacherer, IEEE Trans. Nucl. Sci. **18**, 1105 (1971).